POSTER 5

VENTILATION FLOW ANALYSIS - FLOW VISUALIZATION AND LDA MEASUREMENTS IN WATER SCALE MODELS, VALIDATION OF NUMERICAL RESULTS

J.R. Fontaine, F. Biolley, R. Rapp, J.C. Sérieys
with technical collaboration of J.C. Cunin

Service Thermique, Ventilation
Institut National de Recherche et de Sécurité
Avenue de Bourgogne, B.P. 27
54501 Vandoeuvre Cédex France

1.1. SYNOPSIS

Within the frame of the IEA Annex 20, laboratory and numerical experiments were conducted in order to study the flow within an isothermal parallepipedic testroom (L x W x H = 4.2 m x 3.6 m x 2.5 m). The air is injected through a complex diffuser (made of 84 nozzles) near the ceiling and is evacuated through a rectangular exit just below the inlet.

While other participants to the Annex 20 made measurements on aeraulic testrooms, we used a hydraulic model scaled to the sixth. The parameters were determined according to a Reynolds similitude. For the experimental approach both Laser Doppler Anemometry and flow visualizations were used. Numerical simulations were carried out using the EOL-3d software developed at INRS.

A comparison between experimental results and numerical predictions is presented. Symmetry, air diffuser modelling and low Reynolds number effects are discussed from both numerical and experimental point of views. The numerical predictions are in good agreement with the experimental results.

1.2. LIST OF SYMBOLS

x, y, z	(m)	:	coordinates
X, Y, Z		:	lines in the occupied zone
L	(m)	:	length of the room or scale model
W	(m)	:	width of the room or scale model
H	(m)	:	height of the room or scale model
y'	(m)	:	y coordinate computed from the ceiling
x_0	(m)	:	virtual origin of the jet
δ	(m)	:	thickness of a wall jet
d	(m)	:	diameter of a nozzle
u, v, w	(m/s)	:	velocity components
u', v', w'	(m/s)	:	fluctuating velocity components
U	(m/s)	:	velocity scale
V	(m/s)	:	mean velocity intensity
V_t	(m/s)	:	mean turbulent velocity
σ	(m/s)	:	velocity standard deviation

u_{rm}	(m/s)	:	maximal radial velocity
u_r	(m/s)	:	radial velocity
U_o	(m/s)	:	velocity in the nozzle
U_x	(m/s)	:	velocity boundary condition at the inlet (box model)
T	(s)	:	time scale
ν	(m^2/s)	:	kinematic viscosity
Q	(m^3/s)	:	flowrate
n, n_a, n_w	(h^{-1})	:	renewal time
$K(\theta)$		:	non dimensional function
h		:	non dimensional function
D		:	constant

2.1. INTRODUCTION

Three dimensional ventilation flows modelling in rooms is a fast expanding subject. One of the goals of IEA Annex 20 was to gather different methods to study well defined testcases in order to provide analysis tools to the conceptors. This paper presents two approaches of flow modelling. The first one is based on numerical simulations and discusses several ways of implementing boundary conditions associated to a complex air diffuser. The second one uses hydraulic simulations and represents the testroom by a water model scaled to the sixth. The parameters are determined according to a Reynolds similitude. This method is flexible and well adapted to flow visualizations. For quantitative analysis, mean and turbulent velocity measurements were performed by Laser Doppler Anemometry.

The visualization of the flow was obtained by injecting fluorescein-dyed water through the inlet and enlightening different vertical and horizontal sections of the testroom with a rotating laser beam.

The different techniques used in this work are first described. An analysis of the flow fields based on LDA measurements, flow visualizations and numerical simulations is then presented. The physical relevance of several assumptions usually used in numerical models is finally discussed with reference to the flow visualization results.

2.2. DESCRIPTION OF THE TESTROOM

The testroom (figure 1) (Heikkinen, 1989) is a L x W x H = 4.2 x 3.6 x 2.5 m^3 parallelepiped. It contains one inlet and one outlet. The air is injected into the room through a complex diffuser. The diffuser consists of 4 rows composed by 21 nozzles (diameter 1.2 10^{-2} m and length 1.5 10^{-2} m). The nozzles are on a 0.71 x 0.17 m^2 rectangle. They are oriented toward the ceiling with an angle ϕ = 40°. The air exhaust is located below the inlet. It is a simple 0.3 x 0.2 m^2 rectangle.

2.3. THE WATER SCALE MODEL AND THE HYDRAULIC BENCH

The flow is analyzed experimentally by hydraulic simulation. The testroom is represented by an altuglass model scaled to the sixth. The model and the hydraulic bench are sketched on figure 2 and figure 3. The scale model is placed in a 2.25 x 1.75 x 1 m^3 closed experimental tank (1, figure 2). The front face of the tank is in glass and the bottom in altuglass. A pump (2) sucks the water out of the model and transfers it into a 3 m^3 buffer tank (3). A flowmeter (4) monitors the pump flowrate. The air diffuser is modelised by 4 rows of 21 nozzles of diameters 2 10^{-3} m and lengths 1.5 10^{-2} m that will be referred to as nozzles or grid diffuser.

As it is suggested for the testroom, the nozzles are oriented with an angle of 40° with respect to the horizontal plane (1, figure 3). By conservation of mass, water comes from the surroundings of the model (2) and enters through the diffuser. Before entering, the flow is homogenized by a divergent-convergent system (3) equipped with grids. For flow visualization purposes, a dye (fluorescein) can be added (4) and properly mixed with the water sucked into the divergent-convergent zone.

2.4. EXPERIMENTAL SET-UP

We only considered isothermal conditions (T = 15°C ± 2°C).

Similarity

A Reynolds similarity is used :
$$(Re)_a = (U_0 d/\nu)_a = (U_0 d/\nu)_w = (Re)_w$$

where   a is the subscript for air and w for water ;
         U_0 is the fluid mean speed in the nozzle of diameter d ;
         v is the kinematic viscosity.

The scaling relations are :

d_a/d_w =   6

v_a/v_w ≈   15

length L_a = L_w *   6

time T_a = T_w *   2.4

velocity U_a = U_w *   2.5

flow rate Q_a = Q_w *   90

renewal time n_a = $n_w/2.4$

Measurement points

The velocity measurements were performed for the case $n_a = 3h^{-1}$.

a/   The following measurement lines in the comfort zone were considered :
     . line X parallel to the x axis   :   (y ; z)   =   (1 ; 0)
     . line Y parallel to the y axis   :   (x ; z)   =   (2.2 ; 0)
     . line Z parallel to the z axis   :   (x ; y)   =   (2.2 ; 1)

b/   Some measurement points along the faces of a box surrounding the inlet were added :
     0.   ≤   x   ≤   1.
     2.   ≤   y   ≤   2.5
     1.3   ≤   z   ≤   2.3

Velocity measurements

The three components of the velocity vectors were measured by Laser Doppler Anemometry.

Longitudinal (u) and vertical components (v) were obtained by measurements through the front face of the experimental tank ; longitudinal (u) and transversal (w) components through the bottom face.

Statistical mean velocities u_m and standard deviations $\sigma = \sqrt{u'^2}$ were computed from (N = 3 072) values of instantaneous velocities.

The computations were done in two steps. First, values of u_m and σ were computed. Then all velocity values u such that $|u - u_m| > 6\,\sigma$ were eliminated and new values of u_m and σ were computed with the remaining data. The amplitude of the mean velocity and turbulent velocity were given by :

$$V = (u_m^2 + v_m^2 + w_m^2)^{1/2}$$

$$V_t = (u'^2 + v'^2 + w'^2)^{1/2}$$

Flow visualization

The flow field can be traced by introducing a dye through the inlet (see section 2.3). Laser tomography is used for visualization : a laser beam reflected by a rotating mirror illuminates a section of the flow. The laser light is absorbed and re-emitted by the fluorescein particles. This produces a picture of the flow which can be recorded by photography and video.

The following tests were performed :

Configuration bg
- room and diffuser as described in section 2.2
- $n_a = 1.5\ h^{-1}$ (bg1) ; $n_a = 3\ h^{-1}$ (bg2) ; $n_a = 6\ h^{-1}$ (bg3)

Configuration bs
- room as described in section 2.2
- air diffuser replaced by a slot ($0.71 \times 0.016\ m^2$)
- $n_a = 3\ h^{-1}$

Configuration bb
- room as described in section 2.2
- air diffuser replaced by a basic rectangle ($0.18 \times 0.062\ m^2$)
- $n_a = 3\ h^{-1}$

Configuration bs and bb were visualized because some participants to Annex 20 had done some numerical simulations of the room by replacing the real diffuser by a slot or a basic rectangle of equivalent areas.

2.5. NUMERICAL MODEL

Numerical simulations were carried out with the EOL-3d software which is being developed at INRS. EOL has been specially devised to deal with ventilation flows ; in particular it contains several tools to analyze the results with an industrial hygienist point of view. Given a particular configuration, the user easily enters its geometry and the associated boundary conditions. The software helps to find the appropriate grid and to compute the flow. It offers the possibility of computing local ages of air, local purging flowrates, time evolution of local pollutant concentrations after a sudden contaminant release, local (or global) ventilation efficiencies. The two-dimensional version of the software (EOL-2d) working for both isothermal and non-isothermal flows is available. EOL-3d is still under development.

Mathematical model

The core of EOL is largely inspired by the works of the Imperial College group (Gosman et al, 1976) and of the University of Karlsruhe (Demuren et al, 1987). It solves the usual transport equations for momentum, mass, temperature, pollutant concentration... Because of turbulence, only ensemble average quantities are considered. Eddy viscosity is computed using a k-ε model (Launder et al, 1974). The partial differential equations are transformed into finite differences equations in implicit and conservative form using the hybrid scheme. The SIMPLEC algorithm is used to satisfy continuity.

Modelisation of the air diffuser

The main difficulty of the problem lies in the boundary condition associated to the air diffuser. It is out of the scope of most numerical methods to modelise 84 jets located on a small surface (0.71 x 0.17 m^2) of a room. Indeed the required grids would be too large to be handled by the present computers.

We used the box model method (Nielsen, 1989) which offers the advantage of being general and in principle applicable to any air diffuser.

z = 0 being a symmetry plane of the configuration, the computations can be restricted to a half box. Nevertheless asymmetric solutions may be observed both numerically and experimentally. This fact will be discussed further.

The box model

The boundary condition associated to the air diffuser is replaced by boundary conditions on two vertical faces of a fictive (half) box surrounding the inlet and bounded by the ceiling. The planes are 0.2 m high. One face is located at a distance of 1.0 m from the diffuser wall ; the other face is parallel to the symmetry plane and distant of 0.5 m from it. On each face, only u_x and u_z are imposed; u_z is computed. A boundary condition $u = U_x$ is kept at the inlet considered as a rectangle of dimensions 0.71×0.17 m^2. U_x is such that $n_a = 3$ h^{-1}. The boundary condition along the box can be considered as an added constraint for the flow field. Similar ideas were used by Lemaire et al (1990).

The components u_x and u_z along the box can be obtained from measurements or from scaling laws. We shall only present results for the second case. Indeed the results obtained from experimental data were not very satisfactory. This was due to the fact that in our hydraulic bench it was very difficult to get reliable results very close to the ceiling. The altuglass ceiling produced important light reflections which disturbed the LDA measurements.

Scaling laws were determined by Skovgaard et al. (1990). The flow under the ceiling is the combination of a three-dimensional wall jet and a radial jet. An oblique impinging jet generates a wall jet with different velocity decays in different directions θ (see figure 4).
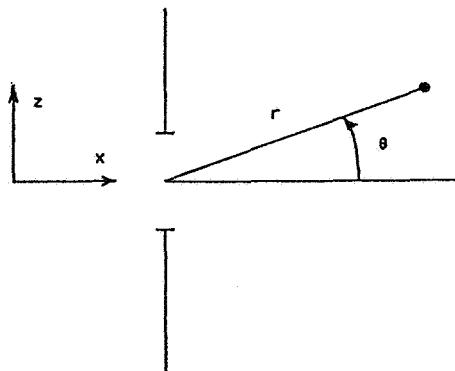
Figure 4 : Definition of coordinates

$$u_{rm}/U_0 = K(\theta) / (r + x_0)$$

with u_{rm} :   maximal radial velocity

      U_0 :   inlet air velocity

      x_0 :   virtual origin

      $K(\theta)$:   angular function

x_0 and $K(\theta)$ are obtained from experiments. u_{rm} being known, the vertical velocity profile close to the ceiling is obtained from wall jet laws :

$$u_r(y') / u_{rm} = h(y'/\delta)$$

$$\delta = D(x_0 + r)$$

h   :   universal function

δ :   boundary layer thickness

$u_r(y')$:   radial velocity at a distance y' from the ceiling (y' = H - y)

D   :   experimental constant

Numerical tests

Three numerical simulations will be discussed.

Simulation S1

Computation for half a room z > 0

$n_a = 3 \ h^{-1}$

Boundary condition : box model

Grid : 32 x 36 x 26

Distances between the last grid points and the wall are all .05 m except for the ceiling where it is .02 m

Simulation S2

Computation for the full room

$n_a = 3 \ h^{-1}$

Boundary condition : box model (full box)

Grid : 27 x 36 x 33

<u>Simulation S3</u>

Computation for the full room

$n_a = 3 \text{ h}^{-1}$

Boundary condition : basic model

Grid : 27 x 36 x 33

In the basic model the real diffuser is replaced by a rectangle (0.18 x 0.062 m^2). The velocity distribution is uniform U_0 is oriented toward the ceiling with an angle $\phi = 40°$. This corresponds to the experimental configuration bb.

S1 has been kept for quantitative comparisons with experiment.

S2 and S3 have been considered to analyze symmetry problems and for comparison with flow visualization experiments.

2.6. RESULTS FOR TEST bg2

<u>Qualitative description of the experiment (flow visualization)</u>

The injected fluid forms a highly turbulent tridimensional jet impinging with an angle on the ceiling (see figures 18 and 20). The jet widens as it flows along the ceiling to the downstream and lateral walls. When it reaches the downstream wall, the fluid spreads out to the sides and the bottom. In short, the jet wraps the testroom.

At the lateral walls near the downstream wall and the ceiling, two streams counteract each other : the one coming from the ceiling in the direction of the main jet and the one bound to the return of the fluid that reached the downstream wall (see figures 20 and 25). Two vertical columns are created in the corners opposite to the diffuser.

Other local features can be observed. First, a small transversal vortex is created in the triangle defined by the jet, the diffuser wall and the ceiling. The vortex rotates in the opposite direction to the main flow circulation and spreads out along the corner. Second, the bottom corners of the diffuser wall present a circulation also opposite to the main flow circulation.

The horizontal sections show that the jet is highly turbulent on the ceiling (see figure 20) but not as much on the bottom (see figure 22).

Quantitative results

The numerical results used in this section are issued from the box model (case S1). The scheme converged after 1 785 iterations and 33 hours of CPU time. The experimental results correspond to the case bg2 : 84 nozzles diffuser and $n_a = 3$ h^{-1}.

Figures 5 and 6 are experimental and numerical tridimensional flow fields respectively. They both show the highest velocities near all but the lateral walls, due to the jet which flows along the walls. Figure 6 is in good agreement with the qualitative description. For example, the columns created by the two currents that counteract each other on the upper corners opposite to the diffuser exist as well in the numerical simulation. However, the small vortex region found experimentally above the jet is not represented numerically due to the choice of the grid or/and the fictive box method.

Figure 7 is a plot of the experimental (dashed line) and numerical (solid line) mean and turbulent velocities on the X, Y and Z lines representative of the comfort zone. In the comfort zone (zone which is at 0.6 m from the vertical walls and up to 1.8 m above the floor), the mean velocities are always less than 0.15 m/s on the X and Z lines. Numerically, the mean velocities can be slightly higher (0.22 m/s) near the floor on line Y.

Predicted and measured data exhibit high turbulent velocities near the ceiling (line Y) as it could be expected from the flow visualizations.

2.7. EXPERIMENTAL STUDY OF SEVERAL SIMPLIFICATIONS INTRODUCED IN THE NUMERICAL SIMULATIONS

In this section, flow visualization will be used as a tool to understand the physical relevance of some simplifications introduced by numericians the perform simulations of complex flow fields. Three phenomena will be studied :
1/ The symmetry hypothesis.
2/ The diffuser modelling.
3/ The high Reynolds number hypothesis.

The symmetry hypothesis

z = 0 is a symmetry plane for all configurations considered in this paper. Indeed both geometry and boundary conditions are the same on both sides of that plane. Therefore, the flow is expected to be symmetric. This explains the fact that most numerical simulations were carried out in half a room (to save computer time).

Both numerical simulations and flow visualizations were conducted for the full room fitted with the real diffuser and with the basic diffuser (rectangle) ; numerical grids were chosen symmetrical with respect to the plane z = 0

Surprisingly enough the results of simulations S2 and S3 are non-symmetrical. Looking at successive horizontal cuts of the flows starting from the ceiling we see that the asymmetry is increasing (figures 14-16 and 15-17). Configurations bb leads to a flow much more asymmetric than configuration bg. This is confirmed by flow visualizations (figures 20-22 and 21-23). We would like to stress the fact that both numerical solutions are fully converged results. This might be explained by the fact that the solutions to the flow equations are non unique and that the resolution algorithms have picked one of the two non symmetrical solutions. Imposing a symmetry condition to the flow at z = 0 presumably leads to an averaging process.

The diffuser modelling

Looking through the numerical results of simulations S2 and S3 we see that in horizontal planes close to the ceiling the flow fields are quite different (figures 14 and 15). For case S2 the air diffuses more in the direction perpendicular to the inlet than in transverse directions. For case S3, we observe the opposite phenomenon. This is confirmed by flow visualizations (figures 20 and 21). This means that the box model is a better approximation of the real diffuser than the basic model.

Looking in a horizontal plane located just above the inlet (y ≈ 2.3 m), we observe from the LDA measurements that the flow induced by the jet enters the lateral faces of the fictive box (figure 13). Even though we have introduced boundary conditions with the fluid flowing out of the box for y ≥ 2.32 m, we see from figure 12 that the flow computed on the plane just below (y = 2.28 m) exhibits fluid motion toward the interior of the box. However, the large velocity measured at the center of the front face of the box was not reproduced by the

numerical simulation. These observations illustrate that the choice of the fictive box to impose boundary condition is quite tricky.

Flow visualizations were also been carried out for the three diffusers (see figures 18, 19 and 24) in vertical planes. The following facts were observed :

1/ The inertia of the jet created by the slot inlet (figure 24) is less than for the two other cases. The jet is inclined to stick much faster to the ceiling and is more influenced by the vortex circulation trapped between the jet, the ceiling and the diffuser wall.

2/ The jet issued from the grid is mainly directed along the x-axis (figure 20) and therefore sticks closer to the ceiling, the downstream vertical wall and the ground (figure 18). For the other jet cases (figures 19 and 24), we observe the opposite phenomenon. The basic jet spreads more in the transversal directions (figure 21) and is thinner on the ceiling in the central plane (figure 19).

Low Reynolds effects

Most computer models use the standard k-ε model of Launder and Spalding (Launder et al, 1974). This model assumes the high Reynolds number hypothesis. This means that viscous effects are negligible compared to fully turbulence effects. In particular, this implies that, after scaling, the flow is Reynolds number independent. In other words this means that the flow field corresponding to $n_a = 3$ h^{-1} can be almost obtained from the case $n_a = 1.5$ h^{-1} by multiplying all velocities by 2. Experimental investigations of Skovgaard et al. have shown that this hypothesis was not satisfied. In this section, we shall use flow visualizations to point out low Reynolds effects.

One manner to discern the low Reynolds effects is to consider the column created by the two countercurrents at the corners opposite to the diffuser wall. Let us consider the x length L_c of the column as defined by figure 25. We should obtain a constant value for the three flowrates if we were at high Reynolds numbers. Figures 25 through 27 are flow visualizations of the front face for increasing Reynolds numbers. It is made clear that the first flowrate has a lower L_c whereas the two others are similar. If this does not demonstrate that the two higher flowrates are similar, it does show that the first flowrate is definitively different from the two others. We are in presence of a low Reynolds effect.

<u>Remark</u>

The flow visualization pictures and numerical flow field map that correspond to each other are listed below.

Numerical simulation   ⇔   Flow visualization

figure 10	⇔	figure 18
figure 11	⇔	figure 19
figure 14	⇔	figure 20
figure 15	⇔	figure 21
figure 16	⇔	figure 22
figure 17	⇔	figure 23

2.8. CONCLUSIONS

In this paper the ventilation of a simple room was investigated by two different methods : numerical simulations and hydraulic simulation. For the hydraulic simulation a model scaled to the sixth was used. The flow was analyzed through LDA measurements and visualization.

Numerical simulations were carried out with the EOL-3d software developed at INRS. The real air diffuser was modelised by using the box model which offers the advantage of being general and applicable to other cases. The comparison between experimental results and numerical predictions is fair and acceptable for industrial purposes.

Hydraulic simulation is well suited to analyze air flow patterns in rooms or premises. It is flexible and well adapted to both LDA measurements and flow visualizations. Indeed it is certainly easier to build scale models than full scale rooms. Moreover performing visualization in a water scale model allows to get a picture of a full plane of the flow at once.

Flow visualization was used as a tool to get some insight into the physics of the flow.
In particular, the influence on the flow of several assumptions such as symmetry, diffuser modelling, high Reynolds number hypothesis, usually used by numericians were pointed out.

60

REFERENCES

1. DEMUREN , A.O., MAJUMDAR, S. and RODI, W.
   "A computer program for solving three-dimensional elliptic flow equations"
   Institüt für Hydromechanik an der Universität Karlsruhe, 1987, unpublished.

2. GOSMAN, A.D. and IDERIAH, F.
   "A general computer program for two-dimensional turbulent recirculating flows"
   Dept of Mech. Eng., Imperial College, London, 1976.

3. HEIKKINEN, J.
   "Specification of testcase B (forced convection, isothermal)"
   Research Item 1.13, IEA Annex 20, Report.

4. LAUNDER, B.E. and SPALDING, D.B.
   "The numerical computation of turbulent flows"
   Comp. Meth. Appl. Mech. Engr., 3, 269, 1974.

5. LEMAIRE, A.D. and ELKHUIZEN, P.A.
   "Simulation of testcase B (forced convection isothermal)"
   IEA Annex 20, report.

6. NIELSEN, P.V.
   "Simplified Models for Room Air Distribution"
   IEA Annex 20, Report, 1989.

7. SKOVGAARD, M., HYLDGAARD, C.E., and NIELSEN, P.V.
   "High and low Reynolds number measurements in a room with an impinging isothermal jet"
   Roomevent Conference, Oslo, 1990.
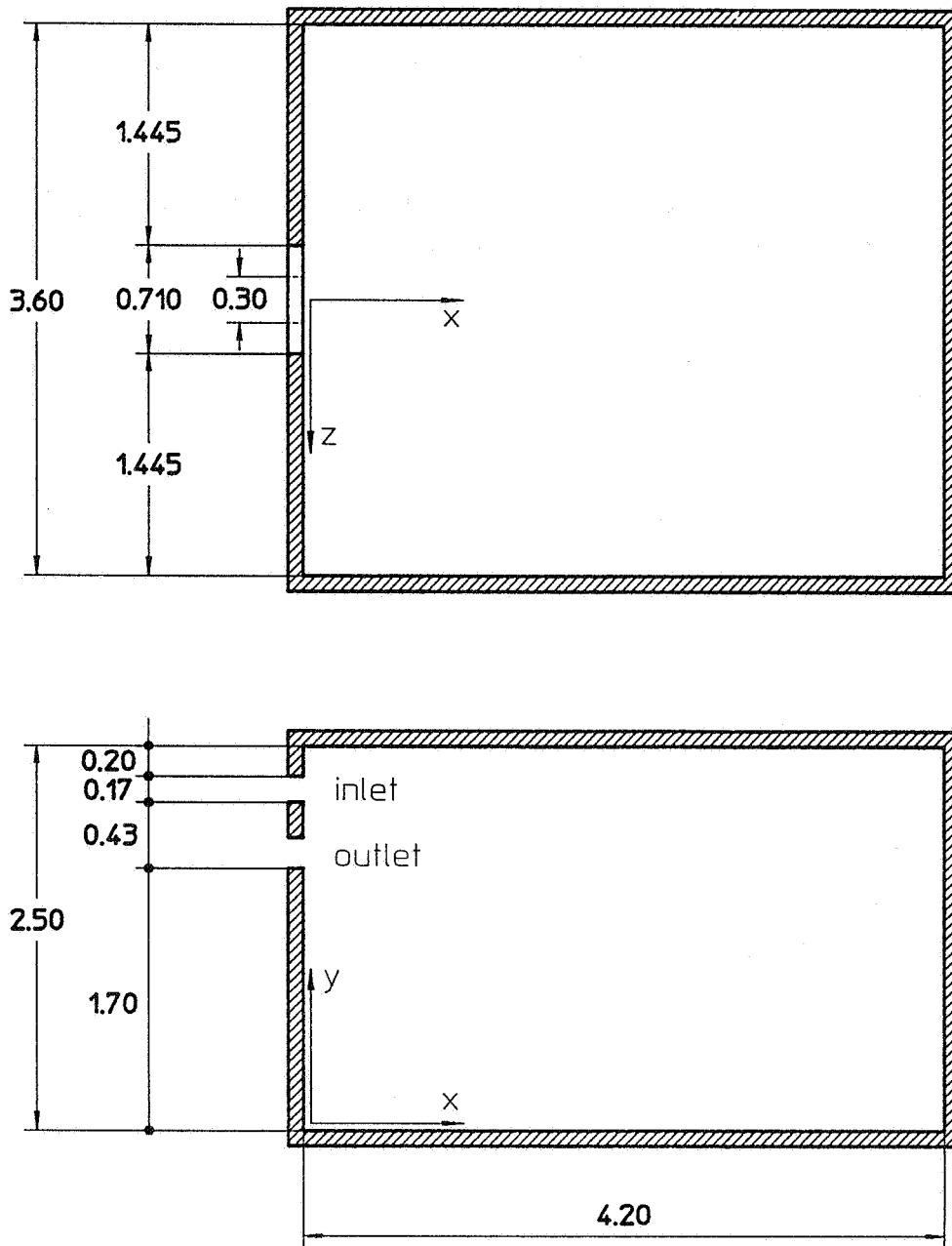
Figure 1 : Testcase b (IEA Annex 20)
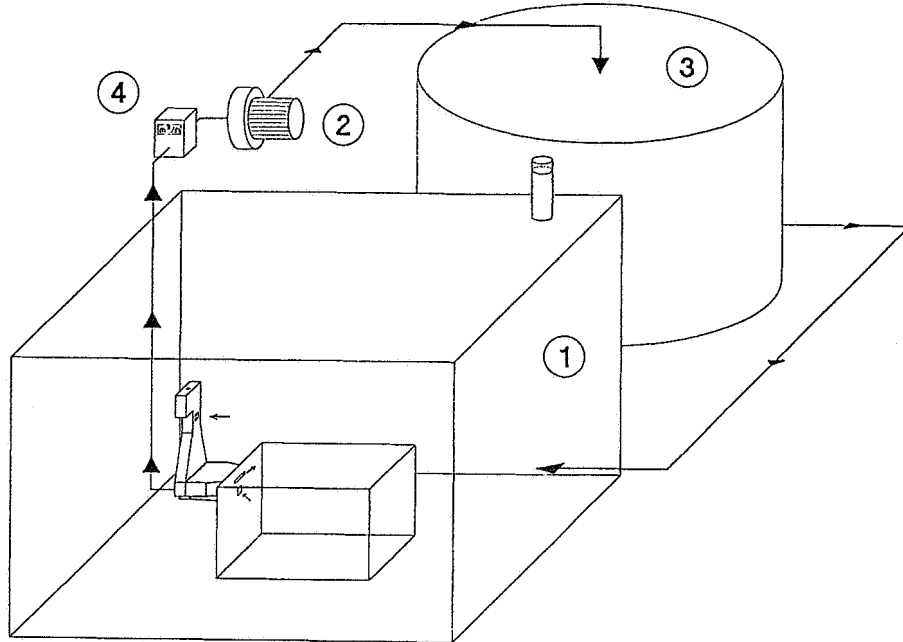
Figure 2 : Sketch of the hydraulic bench
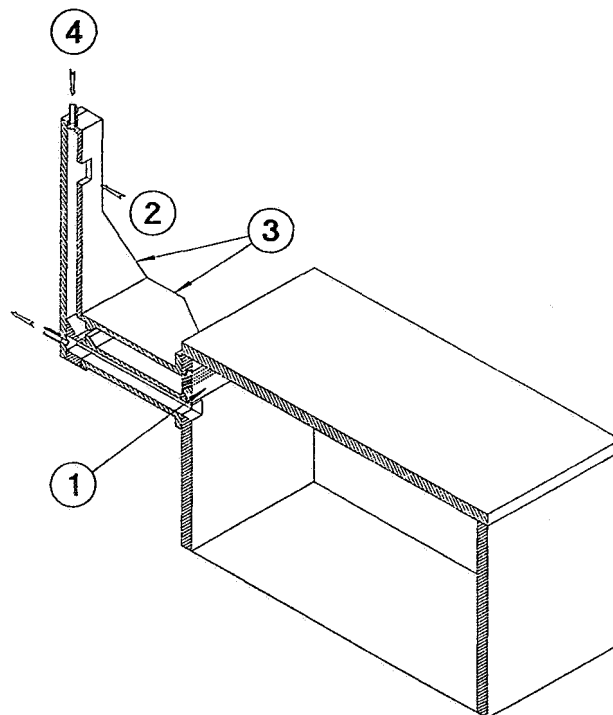
Figure 3 : Testroom model (scale 1/6)
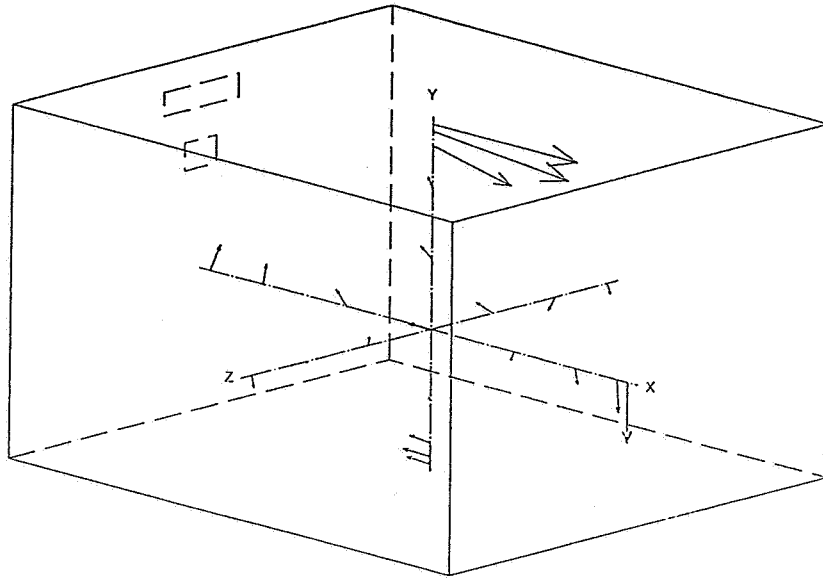
Figure 5 : Three dimensional velocity field obtained from laser anemometry
on lines X, Y, Z ($n_a = 3$ h^{-1})
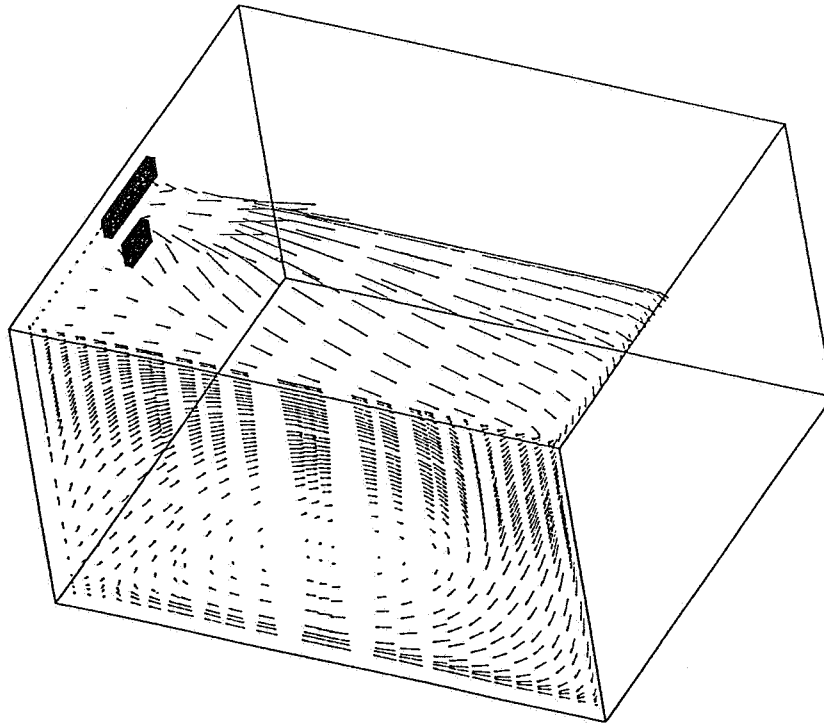
Figure 6 : Three dimensional velocity field obtained from EOL-3d
Simulation S1, $n_a = 3$ h^{-1}

Mean Velocity on the X line

Turbulent velocity on the X line

Mean Velocity on the Y line

Turbulent velocity on the Y line

Mean Velocity on the Z line

Turbulent velocity on the Z line
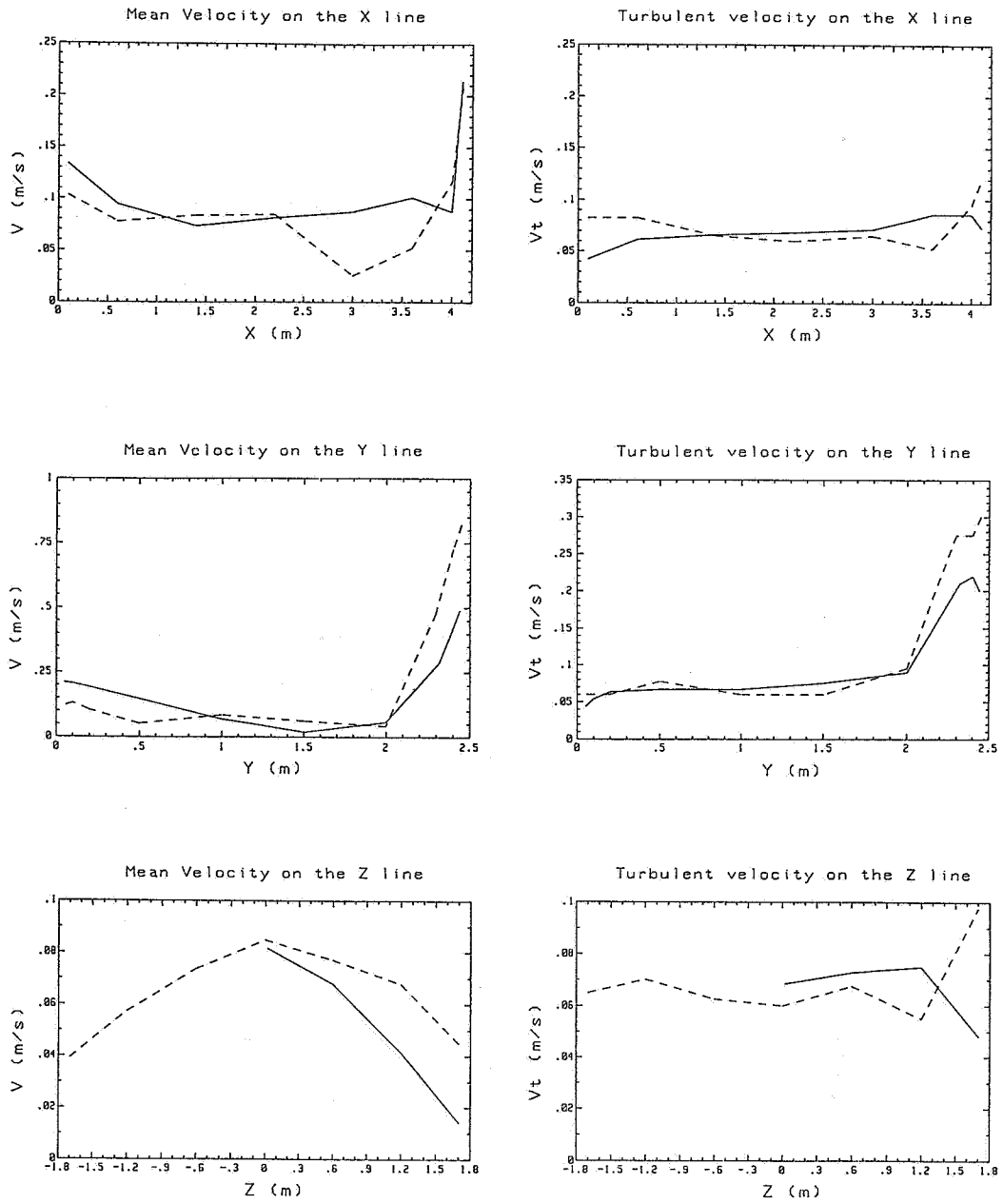
Figure 7 : Mean and turbulent velocities

_____   numerical prediction

-----------   experimental measurements transformed

into air values according to the relations of section 2.4
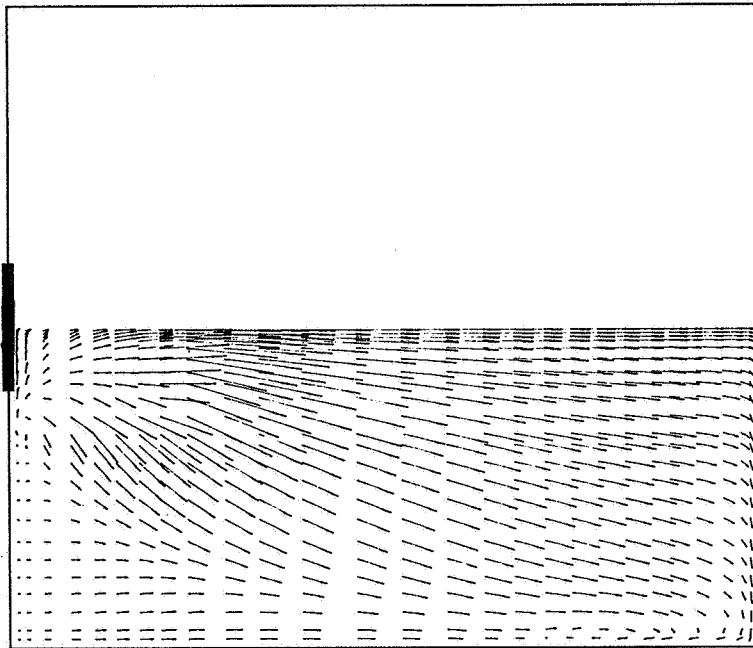
———— 1 m/s

Figure 8 : Horizontal cut of the flow field associated to S1 (y = 2.48 m).
Box model and symmetry assumption ; $n_a = 3$ h^{-1}
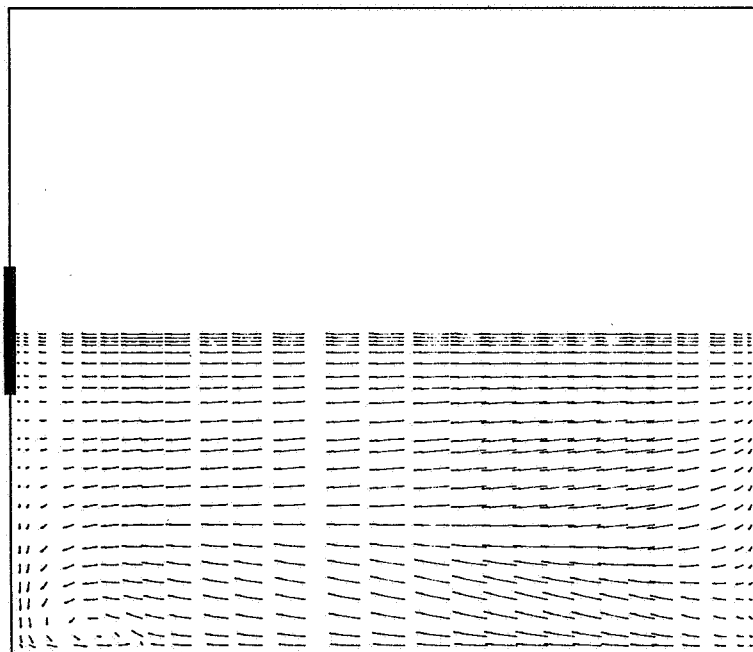
———— 1 m/s

Figure 9 : Horizontal cut of the flow field associated to S1 (y = 0.1 m).
Box model and symmetry assumption ; $n_a = 3$ h^{-1}

1 m/s
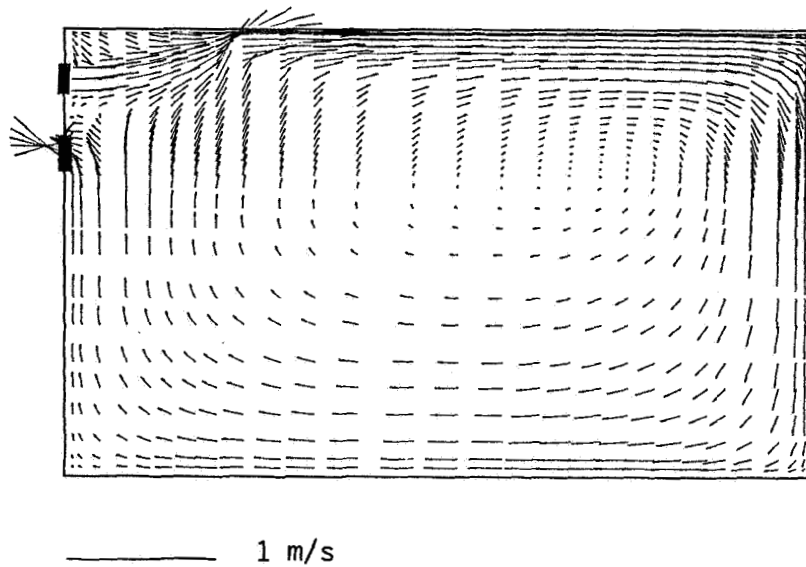
Figure 10 : Vertical cut of the flow field associated to S1 (z = 0.02 m).
Box model and symmetry assumption ; $n_a = 3 \text{ h}^{-1}$

1 m/s
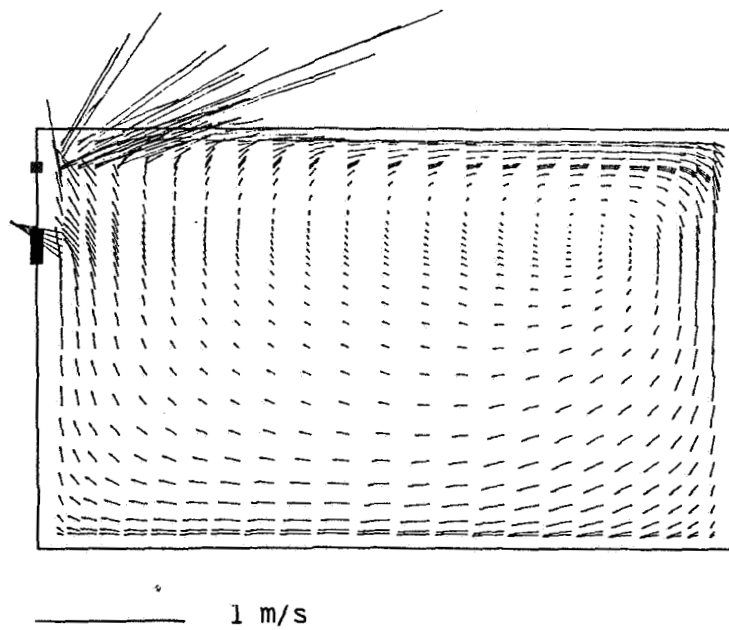
Figure 11 : Vertical cut of the flow field associated to S3 (z = 0.02 m).
Box model, no symmetry assumption ; $n_a = 3 \text{ h}^{-1}$
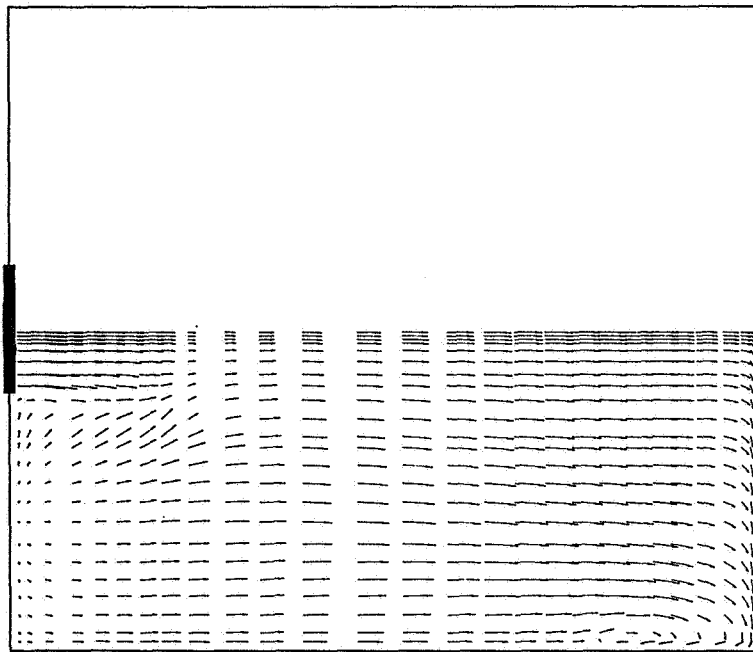
_____ 1 m/s

Figure 12 : Horizontal cut of the velocity field associated to S1 (y = 2.28 m).
Box model and symmetry assumption ; $n_a = 3$ h^{-1}
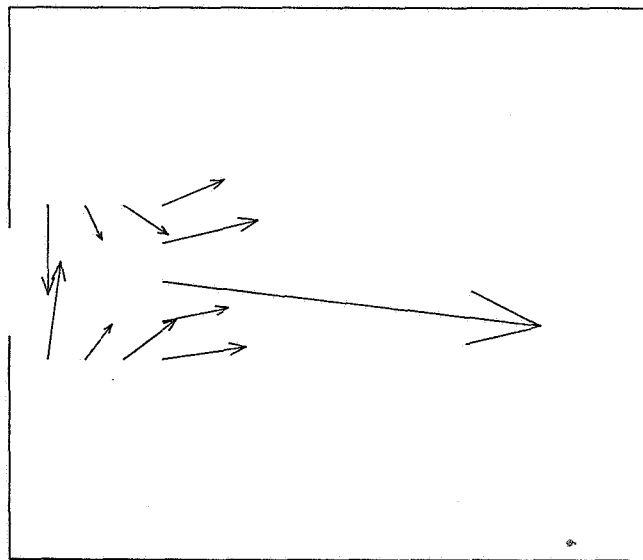
_____ 0.1 m/s

Figure 13 : Horizontal cut of the velocity field associated to bg2
in the vicinity of the air diffuser (y = 2.3 m). LDA measurements for $n_a = 3$ h^{-1}

_____ 1 m/s
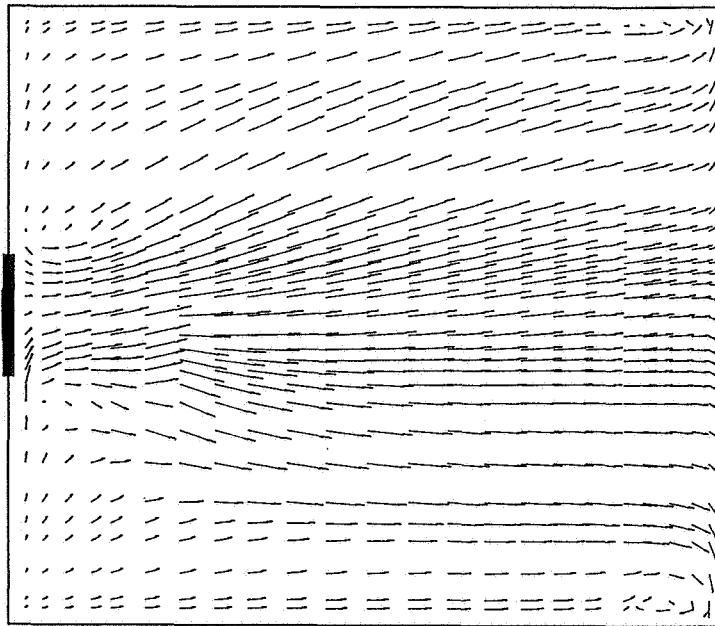
Figure 14 : Horizontal cut of the flow field associated to S2 (y = 2.4 m).
Box model, no symmetry assumption ; $n_a = 3 \, h^{-1}$

_____ 1 m/s
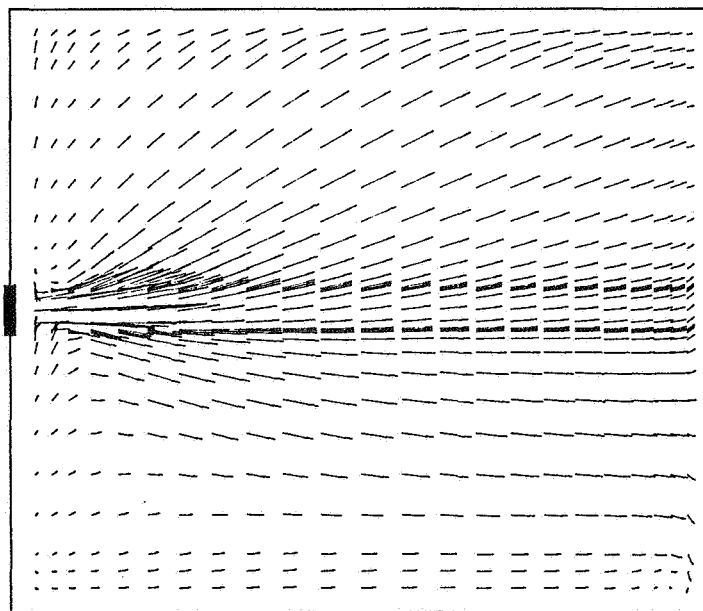
Figure 15 : Horizontal cut of the flow field associated to S3 (y = 2.42 m).
Basic model, no symmetry assumption ; $n_a = 3 \, h^{-1}$

_____ 1 m/s
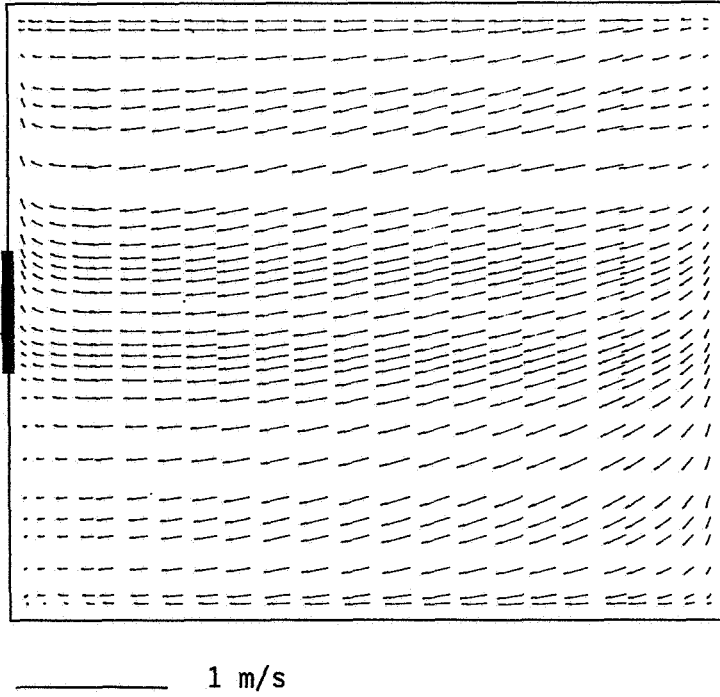
Figure 16 : Horizontal cut of the flow field associated to S3 (y = 0.1 m).
Box model, no symmetry assumption ; $n_a = 3$ h^{-1}

_____ 1 m/s
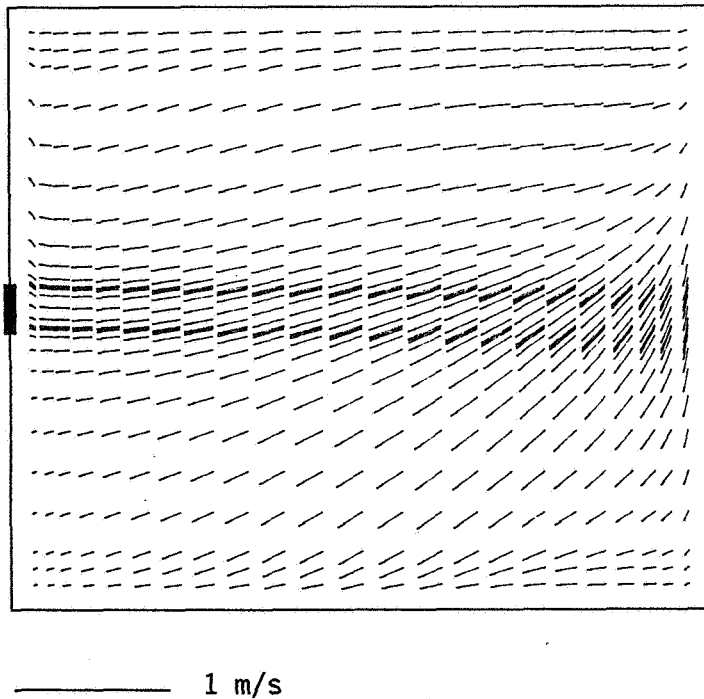
Figure 17 : Horizontal cut of the flow field associated to S3 (y = 0.1 m).
Basic model, no symmetry assumption ; $n_a = 3$ h^{-1}
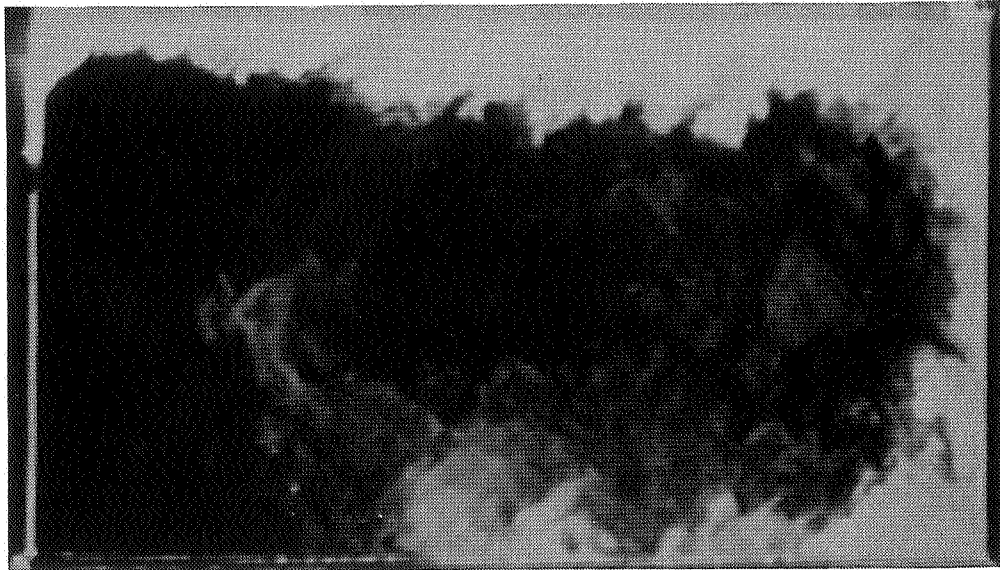
Figure 18 : Flow visualization in the central plane (z = 0 m).
Case bg2, nozzles diffuser ; $n_a = 3$ h^{-1}
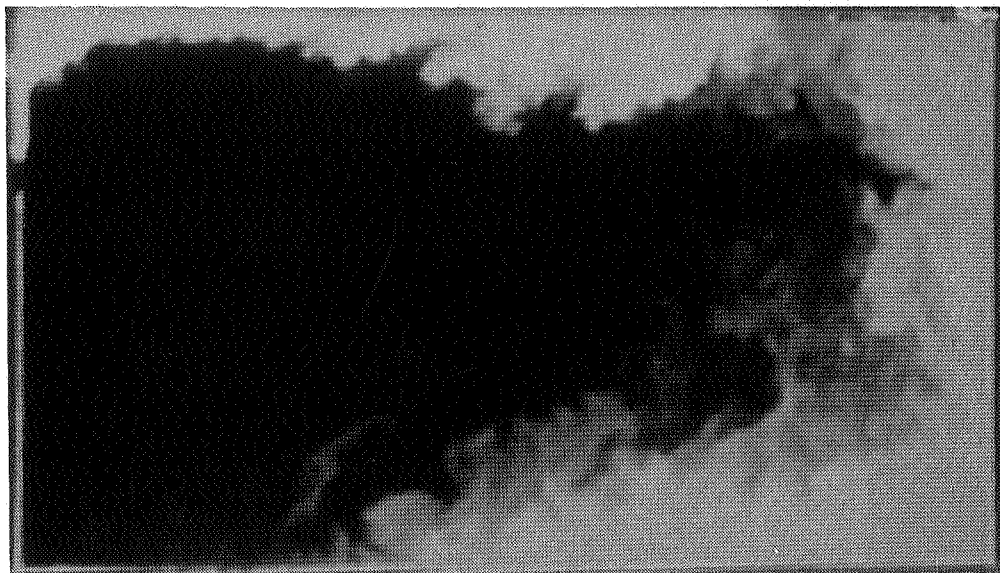
Figure 19 : Flow visualization in the central plane (z = 0 m).
Case bb, basic diffuser ; $n_a = 3$ h^{-1}

Figure 20 : Flow visualization in a horizontal plane
close to the ceiling (y = 2.4 m). Case bg2, nozzles diffuser ; $n_a = 3\ h^{-1}$
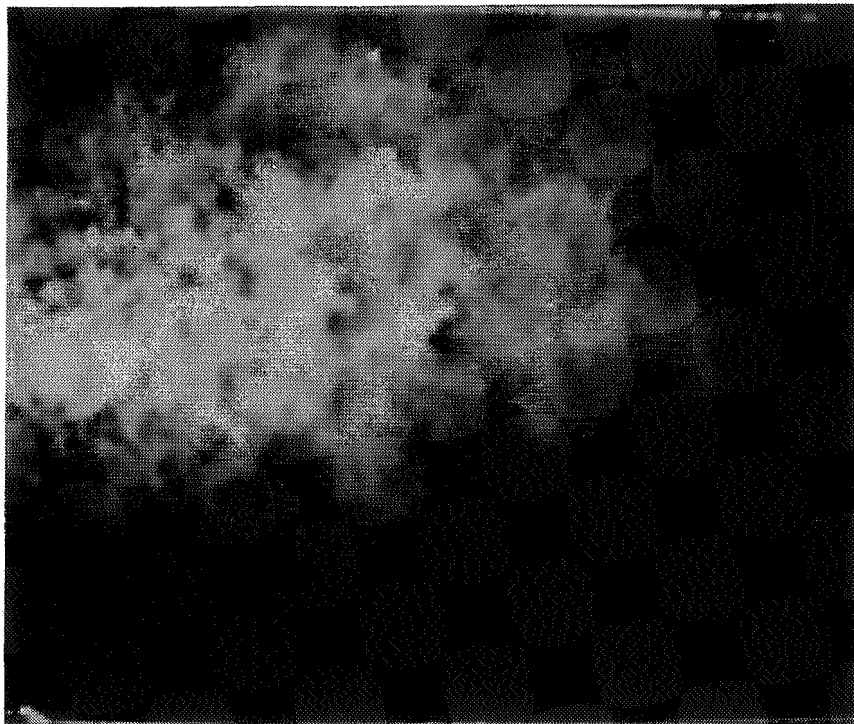
Figure 21 : Flow visualization in a horizontal plane
close to the ceiling (y = 2.4 m). Case bb, basic diffuser ; $n_a = 3\ h^{-1}$
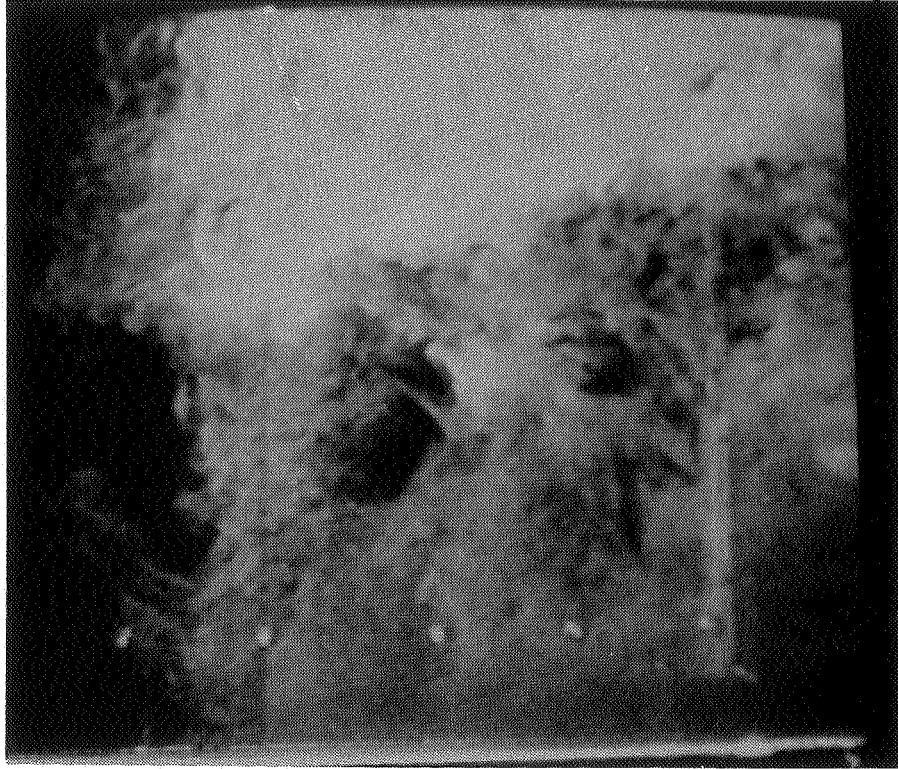
Figure 22 : Flow visualization in a horizontal plane at the bottom (y = 0.1 m).
Case bg2, nozzles diffuser ; $n_a = 3$ h^{-1}
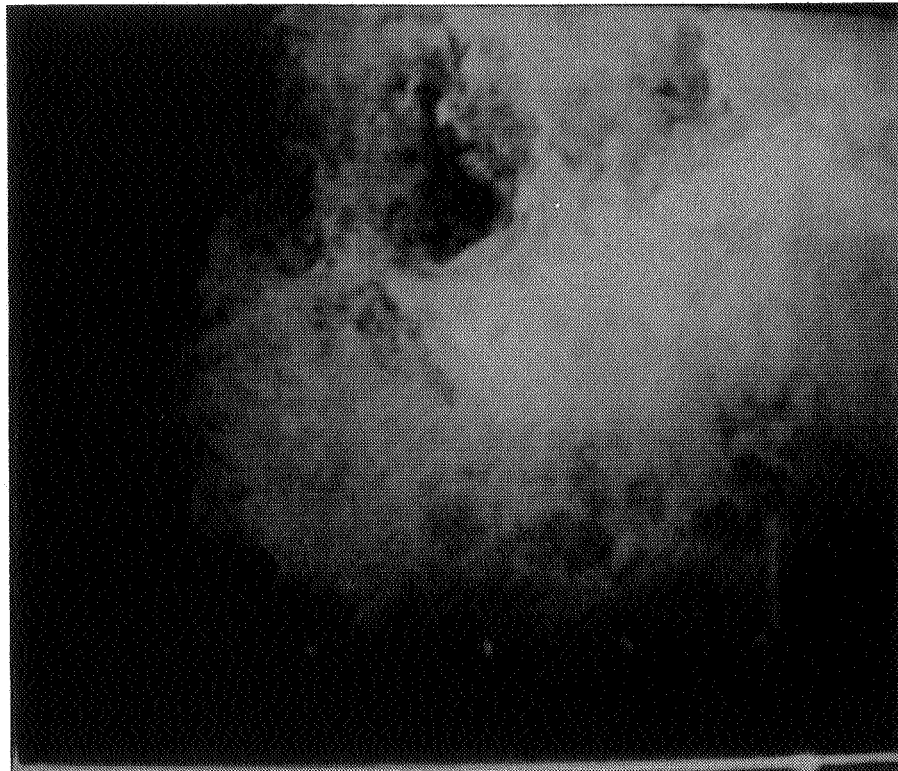
Figure 23 : Flow visualization in a horizontal plane at the bottom (y = 0.1 m).
Case bb, basic diffuser ; $n_a = 3$ h^{-1}
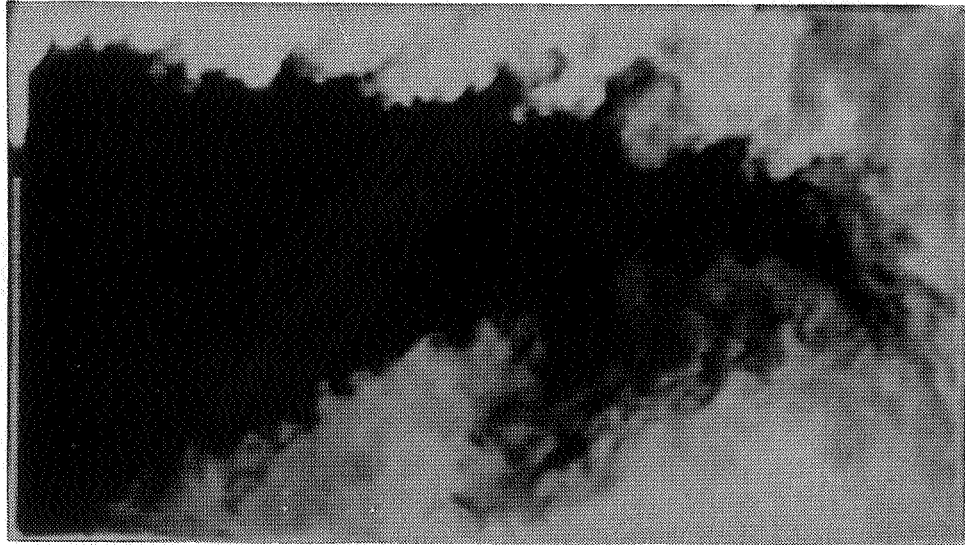
Figure 24 : Flow visualization in the central plane (z = 0 m).
Case bs, slot diffuser ; $n_a = 3$ h^{-1}
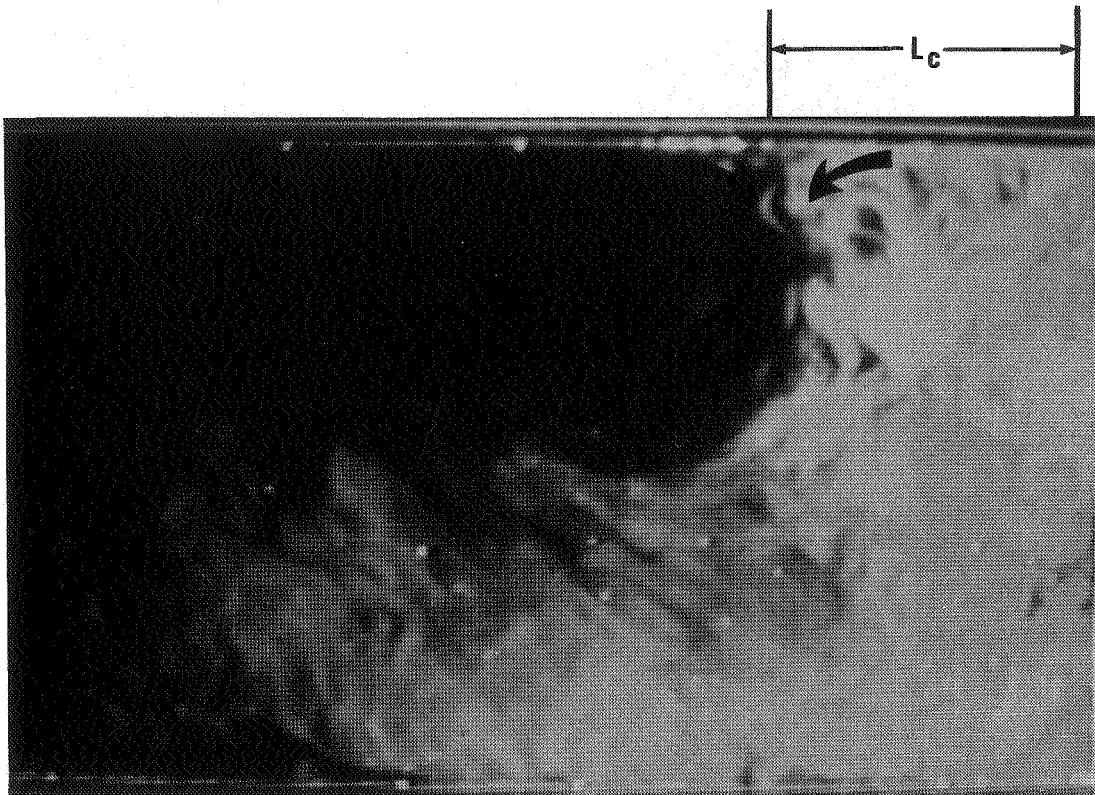
Figure 25 : Flow visualization in the front plane (z = 1.7 m).
Case bg1, nozzles diffuser ; $n_a = 1.5$ h^{-1}
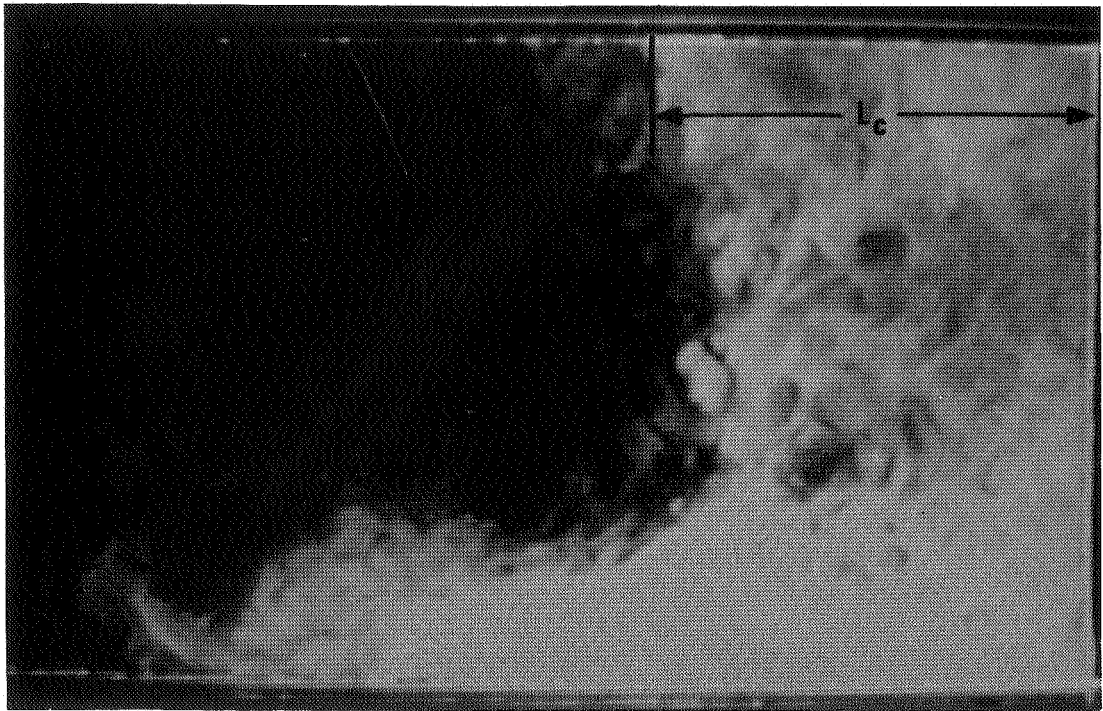
Figure 26 : Flow visualization in the front plane (z = 1.7 m).
Case bg2, nozzles diffuser ; $n_a = 3 \ h^{-1}$
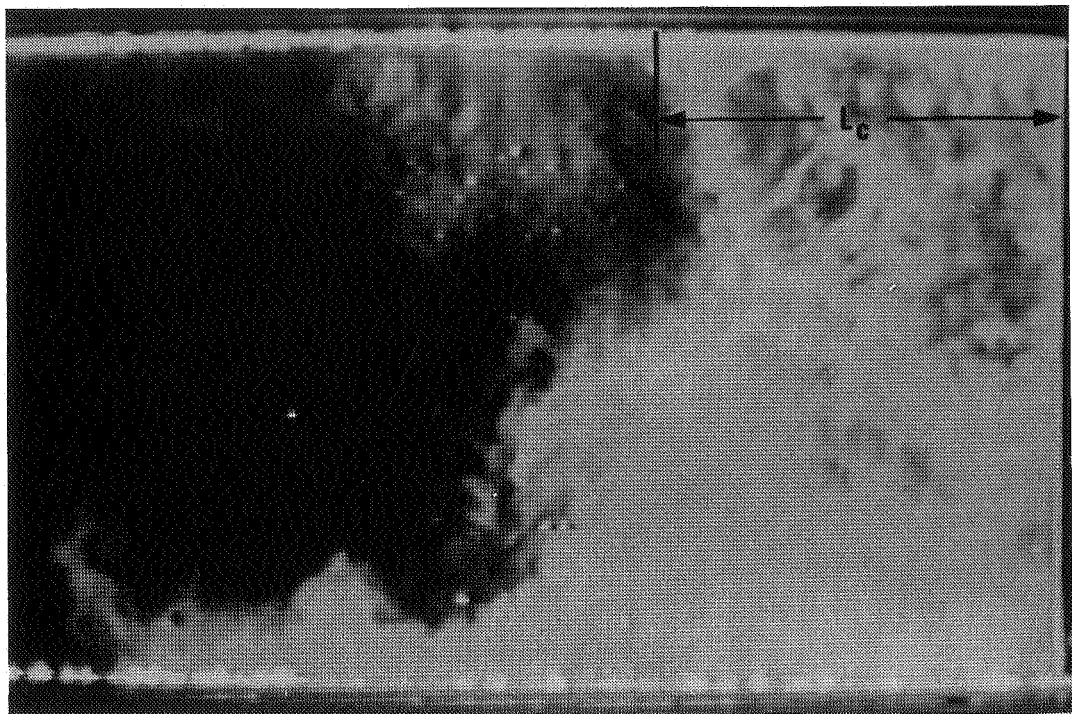
Figure 27 : Flow visualization in the front plane (z = 1.7 m).
Case bg3, nozzles diffuser ; $n_a = 6 \ h^{-1}$